

A new understanding of El Niño's impact over East Asia: dominance of the ENSO combination mode

Article

Accepted Version

Zhang, W., Li, H., Stuecker, M. F., Jin, F.-F. and Turner, A.
ORCID: <https://orcid.org/0000-0002-0642-6876> (2016) A new understanding of El Niño's impact over East Asia: dominance of the ENSO combination mode. *Journal of Climate*, 29 (12). pp. 4347-4359. ISSN 1520-0442 doi: <https://doi.org/10.1175/JCLI-D-15-0104.1> Available at <https://centaur.reading.ac.uk/39366/>

It is advisable to refer to the publisher's version if you intend to cite from the work. See [Guidance on citing](#).

To link to this article DOI: <http://dx.doi.org/10.1175/JCLI-D-15-0104.1>

Publisher: American Meteorological Society

All outputs in CentAUR are protected by Intellectual Property Rights law, including copyright law. Copyright and IPR is retained by the creators or other copyright holders. Terms and conditions for use of this material are defined in the [End User Agreement](#).

www.reading.ac.uk/centaur

CentAUR

Central Archive at the University of Reading

Reading's research outputs online



AMERICAN METEOROLOGICAL SOCIETY

Journal of Climate

EARLY ONLINE RELEASE

This is a preliminary PDF of the author-produced manuscript that has been peer-reviewed and accepted for publication. Since it is being posted so soon after acceptance, it has not yet been copyedited, formatted, or processed by AMS Publications. This preliminary version of the manuscript may be downloaded, distributed, and cited, but please be aware that there will be visual differences and possibly some content differences between this version and the final published version.

The DOI for this manuscript is doi: 10.1175/JCLI-D-15-0104.1

The final published version of this manuscript will replace the preliminary version at the above DOI once it is available.

If you would like to cite this EOR in a separate work, please use the following full citation:

Zhang, W., H. Li, M. Stuecker, F. Jin, and A. Turner, 2015: A New Understanding of El Niño's Impact over East Asia: Dominance of the ENSO Combination Mode. *J. Climate*. doi:10.1175/JCLI-D-15-0104.1, in press.

© 2015 American Meteorological Society



1 **A New Understanding of El Niño’s Impact over East Asia:**
2 **Dominance of the ENSO Combination Mode**

3 **Wenjun Zhang¹, Haiyan Li¹, Malte F. Stuecker², Fei-Fei Jin², Andrew G.**
4 **Turner^{3,4}**

5 ¹*Collaborative Innovation Center on Forecast and Evaluation of Meteorological Disasters, Key*
6 *Laboratory of Meteorological Disaster of Ministry of Education, Nanjing University of*
7 *Information Science and Technology, Nanjing 210044, China*

8 ²*Department of Meteorology, School of Ocean and Earth Science and Technology, University of*
9 *Hawai’i at Manoa, Honolulu, HI 96822, USA*

10 ³*NCAS-Climate, University of Reading, Reading RG6 6BB, UK*

11 ⁴*Department of Meteorology, University of Reading, Reading RG6 6BB, UK*

12 *Sep. 12, 2015*

13 *(2th Revision for J. Clim.)*

14

15 *Corresponding author address:*

16 Dr. Wenjun Zhang
17 College of Atmospheric Sciences, Nanjing University of Information
18 Science and Technology, Nanjing 210044, China.
19 E-mail: zhangwj@nuist.edu.cn

20

Abstract

21

22 Previous studies have shown that the Indo-Pacific atmospheric response to
23 ENSO comprises two dominant modes of variability: a meridionally quasi-symmetric
24 response (independent from the annual cycle) and an anti-symmetric response (arising
25 from the nonlinear atmospheric interaction between ENSO variability and the annual
26 cycle), referred to as the combination mode (C-Mode). This study demonstrates that
27 the direct El Niño signal over the tropics is confined to the equatorial region and has
28 no significant impact on the atmospheric response over East Asia. The El
29 Niño-associated equatorial anomalies can be expanded towards off-equatorial regions
30 by the C-Mode through ENSO's interaction with the annual cycle. The C-Mode is the
31 prime driver for the development of an anomalous low-level anticyclone over the
32 western North Pacific (WNP) during the El Niño decay phase, which usually
33 transports more moisture to East Asia and thereby causes more precipitation over
34 southern China. We use an Atmospheric General Circulation Model that well
35 reproduces the WNP anticyclonic anomalies when both El Niño sea surface
36 temperature (SST) anomalies as well as the SST annual cycle are prescribed as
37 boundary conditions. However, no significant WNP anticyclonic circulation anomaly
38 appears during the El Niño decay phase when excluding the SST annual cycle. Our
39 analyses of observational data and model experiments suggest that the annual cycle
40 plays a key role in the East Asian climate anomalies associated with El Niño through
41 their nonlinear atmospheric interaction. Hence, a realistic simulation of the annual
42 cycle is crucial in order to correctly capture the ENSO-associated climate anomalies

43 over East Asia.

44 **1. Introduction**

45 The El Niño–Southern Oscillation (ENSO) is an irregular fluctuation between
46 warm (El Niño) and cold (La Niña) conditions in sea surface temperature (SST) over
47 the central and eastern tropical Pacific, arising from large-scale ocean-atmosphere
48 interactions (e.g., Bjerknes 1969; Neelin et al. 1998; Wallace et al. 1998). There is
49 widespread public concern since ENSO gives rise to pronounced climate anomalies
50 around the globe (e.g., van Loon and Madden 1981; Ropelewski and Halpert 1987,
51 1996; Trenberth and Caron 2000; Alexander et al. 2002). The significant circulation
52 and precipitation anomalies associated with ENSO provide a potential source of
53 predictability for forecasting regional climate anomalies on seasonal-to-interannual
54 timescales, especially in the tropics (e.g. Charney and Shukla 1981).

55 East Asia is inhabited by approximately one-third of the global population, and
56 ENSO has been demonstrated to strongly modulate its climate (e.g., Fu and Teng
57 1988; Huang and Wu 1989; Zhang et al. 1996; Wang et al. 2000, 2013; Wu and Hu
58 2003; Lau and Nath 2006, 2009; Wu et al. 2009; Zhang et al. 2014). Positive
59 precipitation anomalies appear commonly over the East Asian polar front extending
60 northeastward from southern China towards southern Japan during boreal spring and
61 early summer of the El Niño decay phase (e.g., Zhang et al. 1996; Wang et al. 2000).
62 The low-level anticyclonic circulation anomalies over the western North Pacific
63 (WNP) serve as a major mediator linking SST anomalies over the eastern tropical
64 Pacific and precipitation anomalies over East Asia (e.g., Harrison and Larkin 1996;
65 Zhang et al. 1996; Wang et al. 2000). The anomalous WNP anticyclone usually starts

66 developing during the ENSO mature phase from boreal late autumn to winter and
67 tends to reach its peak in the following spring season (e.g., Harrison and Larkin 1996;
68 Wang et al. 2000, 2002, 2013). Since strong SST anomalies can be directly observed
69 during the El Niño development, these can serve as an early indicator for subsequent
70 precipitation and circulation anomalies to appear over East Asia.

71 Several dynamical mechanisms were proposed to address how ENSO affects the
72 WNP atmospheric circulation. Diagnostic analyses by Zhang et al. (1996) suggested
73 that the WNP atmospheric circulation anomalies are induced by suppressed
74 convection over the western equatorial Pacific due to a weakened Walker circulation
75 during El Niño. Wang et al. (2000) argued that cold SST anomalies over the western
76 tropical Pacific favor the occurrence of the anomalous WNP anticyclone as a
77 Rossby-wave response (Matsuno 1966; Gill 1980). This anomalous anticyclone can
78 persist until early summer after the El Niño peak phase, due to a positive feedback
79 between local surface wind and SST anomalies (wind-evaporation-SST feedback)
80 (e.g., Wang et al. 2000). However, this mechanism was challenged by recent studies
81 (e.g., Yang et al. 2007; Xie et al. 2009), in which the delayed Indian Ocean warming
82 after the El Niño peak months was identified as playing an important role in the
83 development of the anomalous anticyclone over the WNP. The delayed Indian Ocean
84 warming can give rise to equatorial surface easterly wind anomalies and suppressed
85 convection in the WNP region through a baroclinic atmospheric Kelvin wave
86 response, thereby establishing the anomalous WNP anticyclone. This argument is
87 supported by several modeling experiments (e.g., Wu and Liu 1995; Watanabe and Jin

88 2002, 2003; Annamalai et al. 2005; Li et al. 2005; Wu et al. 2010). A recent study
89 hypothesized that the delayed Indian Ocean warming is not able to fully explain the
90 observed meridionally anti-symmetric atmospheric responses over the Western Pacific
91 since the atmospheric Kelvin wave response is symmetric about the equator (Stuecker
92 et al. 2015). So far, the fundamental dynamical mechanisms responsible for the
93 ENSO-related climate anomalies over East Asia are still controversial and deserve
94 further study.

95 As one of the latest advances in ENSO research, the so-called combination mode
96 (C-Mode) is found to occur in the Indo-Pacific region, resulting from the nonlinear
97 atmospheric interaction between the annual cycle and ENSO variability (Stuecker et
98 al. 2013, 2015). The C-Mode encompasses both the southward shift of low-level
99 zonal wind anomalies over the central Pacific and the development of strong
100 low-level anti-cyclonic circulation anomalies over the WNP during the peak and
101 decaying El Niño phases in boreal winter and spring. The southward shift of zonal
102 surface wind anomalies is attributed to the meridional seasonal march of Western
103 Pacific background warm SSTs following the maximum in solar insolation (e.g.,
104 Harrison 1987; Harrison and Larkin 1998; Harrison and Vecchi 1999). The circulation
105 anomalies associated with this are shown to accelerate El Niño event terminations by
106 allowing the thermocline to adjust upwards towards a normal state in the eastern
107 Pacific (Harrison and Vecchi 1999; Kug et al. 2003; Vecchi and Harrison 2003, 2006;
108 Spencer 2004; Lengaigne et al. 2006; Ohba and Ueda 2009; McGregor et al. 2012,
109 2013). As an important part of the C-Mode, strong anticyclonic low-level circulation

110 anomalies develop over the WNP, leading to greater fluxes of moisture towards East
111 Asia (e.g., Stuecker et al. 2013, 2015). The annual cycle modulation is demonstrated
112 to play a key role on the ENSO associated atmospheric circulation and precipitation
113 response over the WNP based on idealized model experiments and a case study for the
114 1997/98 El Niño episode (Stuecker et al. 2015), and hence is expected to make a
115 dominant contribution to climate anomalies over East Asia. At present, it is unclear to
116 what extent the annual cycle affects East Asian climate anomalies associated with
117 ENSO in the observations, since little attention has been paid to it. This scientific
118 issue deserves study in order to deepen our understanding of the mechanism by which
119 ENSO affects East Asian climate.

120 In this study, the role of the annual cycle in ENSO-related climate impacts over
121 East Asia will be investigated through analyses of observational data and numerical
122 model experiments. It is our hypothesis that the annual cycle plays a predominant role
123 in East Asian climate anomalies through its interaction with ENSO variability
124 predominantly during the ENSO decaying phase. In the remainder of the paper,
125 section 2 introduces the data used, methodology, and experimental information.
126 Section 3 illustrates the linkage of the ENSO mode and the associated C-Mode to the
127 WNP atmospheric anomalies and thus East Asian climate anomalies. In section 4, we
128 describe the model experiments utilized to further investigate the effects of the annual
129 cycle on the ENSO-associated climate anomalies over East Asia. The major findings
130 and discussion are summarized in section 5.

131

132 **2. Data, Methodology, and Experimental design**

133 **a. Data and Methodology**

134 The monthly 160-station gauge-based precipitation data (1961-2012) used here
135 were supplied by the China Meteorological Administration. The leading wind modes
136 associated with ENSO and the associated atmospheric circulation were investigated
137 based on the National Centers for Environmental Prediction/National Center for
138 Atmospheric Research (NCEP-NCAR) reanalysis (Kalnay et al. 1996). The SST data
139 (1961–2012) were examined based on the global sea ice and sea surface temperature
140 analyses from the Hadley Centre (HadISST1) provided by the Met Office Hadley
141 Centre (Rayner et al. 2003). Monthly anomalies were derived relative to a 30-year
142 climatological mean (1971–2000), and then a 6–120-month band-pass filter was
143 applied to each dataset since the ENSO interannual and C-Mode near-annual
144 variability are our focus. Our conclusions remain unchanged when using the
145 unfiltered data.

146 Composite and linear regression analyses were employed to analyze possible
147 impacts of ENSO and the related C-Mode on the climate of East Asia. Partial
148 correlations/regressions between atmospheric fields and the ENSO or the C-Mode are
149 used to remove the linear influence from each other by keeping the respective other
150 index unchanged (e.g. Ashok et al. 2007). The statistical significance of our results is
151 inferred using a two-sided Student's *t*-test. The following eight strongest El Niño
152 events in the available record are defined by the climate prediction center using a
153 threshold of 0.5°C for the Niño-3.4 region (5°S–5°N, 120°–170°W) area-averaged

154 SST anomalies: 1965/66, 1968/69, 1972/73, 1982/83, 1986/87, 1991/92, 1997/98, and
155 2009/10. To detect a robust signal, strong warming events only are selected given that
156 the circulation anomalies associated with strong C-Mode events usually accompany
157 strong El Niño events (McGregor et al. 2012, 2013; Stuecker et al. 2013). Even when
158 all El Niño events are chosen for our composite analysis, the main conclusions remain
159 unchanged, albeit with a relatively weakened atmospheric response.

160 It is notable that climate anomalies over East Asia display strong seasonal
161 differences during El Niño conditions. As an example, significant precipitation
162 anomalies occur over southern China during El Niño decaying spring seasons (e.g.,
163 Zhang et al. 1999; Wang et al. 2000). Nevertheless, the climate signal of El Niño over
164 eastern China is difficult to detect in summer season during its decay (e.g., Zhang et al.
165 1999; Wang et al. 2000), although more moisture is clearly brought to East Asia from
166 the tropical oceans. This non-stationary behavior is possibly associated with some
167 other modulating factors such as Tibetan Plateau snow cover and land surface
168 conditions over Eurasia, strongly influencing the East Asian summer monsoon (e.g.,
169 Ye 1981; Tao and Ding 1981; Zhang et al. 2004; Wu and Kirtman 2007; Wang et al.
170 2008; Wu and Qian 2010; Wu et al. 2012). In this study, the El Niño decaying months
171 from February to May (FMAM) are our focus since the land precipitation anomalies
172 are most evident during this season in China. The “decaying months” can also be
173 defined by MAM (March to May), and even MAMJ (March to June) or FMAMJ
174 (February to June), and the qualitative conclusions remain the same.

175

176 **b. Experimental information**

177 To examine the role of the annual cycle in modulating ENSO impacts over East
178 Asia, two sets of experiments are conducted based on the GFDL Atmospheric General
179 Circulation Model (AGCM) AM2.1 with a horizontal resolution of 2.5° longitude \times 2°
180 latitude with specified SST boundary conditions (the GFDL Global Atmospheric
181 Model Development Team 2004). The specific experimental designs will be shown in
182 Section 4, which has also been described in the supplementary materials of Stuecker
183 et al. (2013).

184

185 **3. Observed analyses for linkage of ENSO and C-Mode to the East**

186 **Asian climate**

187 We perform an empirical orthogonal function (EOF) analysis, as in previous
188 studies (McGregor et al. 2012, 2013; Stuecker et al. 2013), on the surface wind
189 anomalies over the equatorial Pacific (10°S – 10°N , 100°E – 80°W) to detect the spatial
190 and temporal wind structures associated with ENSO and the C-mode. Figure 1 shows
191 the leading two EOF modes and their associated principal components (PCs). The
192 leading two modes, respectively, account for 23.1% and 18.0% of the total variance,
193 and are well separated from each other based on the rule of North et al. (1982). The
194 typical ENSO mode wind anomaly pattern is captured by the leading EOF mode
195 (EOF1), which exhibits equatorially quasi-symmetric westerly wind anomalies
196 occurring over the central Pacific (Fig. 1a). A high correlation ($r=0.87$) between the
197 Niño3.4 index and PC1 further confirms that the first EOF mode represents the direct

198 atmospheric response associated with ENSO. Compared to EOF1, the EOF2 wind
199 anomaly pattern displays meridionally anti-symmetric wind anomalies (Fig. 1b). An
200 anomalous anticyclone is located over the WNP and a cyclonic meridional shear of
201 wind anomalies occurs over the central South Pacific. This wind anomaly pattern is
202 referred to as the C-Mode and arises from the interaction between the annual cycle
203 and interannual ENSO variability (Stuecker et al. 2013, 2015). The PC2 time series
204 can be well reconstructed by using a product of PC1 and the annual cycle of the
205 western Pacific SSTs, as documented by Stuecker et al. (2013). The direct ENSO
206 circulation response therefore does not include the characteristic pattern of the
207 anomalous WNP anticyclone (Fig. 1a), the key mediator linking the tropical eastern
208 Pacific warming and the climate anomalies over East Asia. The WNP anticyclonic
209 circulation anomalies depicted by EOF2 suggest that the annual cycle plays a key role
210 modulating ENSO climate impacts over East Asia. We will demonstrate this
211 hypothesis in the remainder of the paper.

212 Figure 2 shows the seasonal evolution of surface wind PC1 and PC2 during the El
213 Niño events. The composite PC1 describes a canonical El Niño evolution, with
214 anomalies developing in summer, peaking during late autumn or winter, and decaying
215 in the following spring. Following the traditional definition, we choose the winter
216 (DJF) mean PC1 values to investigate the impacts of PC1 on the following seasonal
217 climate anomalies over East Asia. In contrast to PC1, PC2 remains negative until
218 September of the El Niño developing year and then reverses its sign abruptly (Fig. 2).
219 It reaches its peak during late winter and early spring, capturing a strong southward

220 shift of the central Pacific westerly anomalies and the development of the WNP
221 circulation anomalies (McGregor et al. 2012). PC2 enters its decaying phase during
222 summer and early autumn following the El Niño mature phase. Compared to PC1, the
223 peak phase of PC2 is delayed by approximately two to three months and it exhibits
224 much faster timescales (for a discussion of the near-annual timescale see Stuecker et
225 al. 2013, 2015). Here, the season JFM is defined as the PC2 mature phase and the
226 JFM mean is used as a measure of the C-Mode to detect its linkage to East Asian
227 climate during the El Niño decaying phase. It is noted here that other possible
228 definitions for the mature phases of PC1 and PC2, e.g., by including the adjacent
229 months, do not alter our conclusions.

230 To detect possible ENSO impacts on precipitation changes, Figure 3a shows the
231 FMAM precipitation anomalies regressed on the preceding DJF average PC1. In this
232 study, the region of eastern China is shown as an example to illustrate the ENSO
233 impacts on the East Asian precipitation. Following El Niño events, eastern China
234 usually receives enhanced precipitation during its decaying phase, especially for the
235 southern part approximately south of 35°N and east of 110°E. Furthermore, the
236 composite precipitation anomalies over the period 1961-2012 are computed during
237 eight strong El Niño events to confirm robustness of the precipitation response. As
238 shown in Figure 3b, similar precipitation anomalies are evident over eastern China
239 (east of 105°E) despite the statistically significant anomalies being confined to
240 southeastern China. Recently, another type of El Niño (the so-called central Pacific El
241 Niño; or CP El Niño) is argued to occur more frequently over the central tropical

242 Pacific in the post-2000 period, which exhibits very different climate impacts over
243 East Asia (Larkin and Harrison 2005; Ashok et al. 2007; Weng et al. 2007; Kao and
244 Yu 2009; Kug et al. 2009; Yeh et al. 2009; Feng et al. 2010; Ren and Jin 2011; Zhang
245 et al. 2011, 2013; Feng and Li 2011; Xie et al. 2012, 2013, 2014; Karori et al. 2013;
246 Xiang et al. 2013; Yuan et al. 2013; Wang and Wang 2013). We further inspect the
247 precipitation composite for the canonical El Niño events (i.e., eastern Pacific El Niño)
248 to test if this El Niño diversity might bias our analysis. Almost the same El Niño
249 signal occurs in the precipitation over southeastern China when we remove the CP
250 events (not shown). Even for CP El Niño events, such as the 1991/92 and 2009/10
251 event, similar positive precipitation anomalies are also evident in this region (not
252 shown). These results suggest that El Niño events are usually accompanied by
253 increased precipitation over eastern China, which has been mentioned by many earlier
254 studies (e.g., Zhang et al. 1999; Wang et al. 2000).

255 Figure 4 shows the correlation and partial correlation between the JFM PC1 and
256 the FMAM precipitation anomalies to detect the pure impacts of PC1. As in Figure 4a,
257 a statistically significant positive correlation is observed over southeastern China
258 between the FMAM precipitation anomalies and the JFM PC1. The correlation
259 coefficients obtain values as high as 0.5. However, almost no significant correlation is
260 detected in this region after removal of the effects of PC2 for a partial correlation (Fig.
261 4b). The correlation and partial correlation techniques are also utilized to distinguish
262 the impact of the C-Mode (PC2) from the ENSO mode (PC1). A statistically
263 significant positive correlation between the C-Mode and the precipitation anomalies is

264 detected over southeastern China (Fig.5a), which is not contaminated by the ENSO
265 mode signal (Fig. 5b). These statistical relations suggest that the ENSO SST forcing
266 itself is not able to produce more precipitation over southeastern China and its
267 impacts on precipitation over southeastern China are only conveyed via the C-Mode
268 through the interaction of ENSO with the annual cycle. To further confirm those
269 results, the FMAM rainfall variability is reconstructed using the simultaneous PC1
270 and PC2 information (Fig. 6). Almost no obvious precipitation variability is explained
271 by the PC1 time series alone. However, in excess of 30% of variance can be explained
272 when further considering the PC2 time series. This highlights the importance of the
273 C-Mode.

274 The atmospheric teleconnection is also examined here to understand possible
275 links between precipitation anomalies over eastern China and the two leading modes
276 (i.e., ENSO mode and the C-Mode). For the ENSO mode, there is an anomalous
277 eastward moisture transport located on the equator, causing more precipitation over
278 the central to eastern equatorial Pacific (Fig. 7a). The moisture transport anomalies
279 are mainly induced by the meridionally quasi-symmetric CP westerly wind anomalies
280 during El Niño events (Fig. 1a). No statistically significant atmospheric anomaly
281 occurs over the WNP (Fig. 7a). When zonally averaging the meridional circulation
282 over 110°-120°E, one finds strong sinking motion over the equatorial western Pacific
283 due to a weakened Walker Circulation for the ENSO mode (Fig. 8a). In contrast to the
284 ENSO mode, significant moisture transport anomalies associated with the C-Mode
285 appear over the WNP region and the central South Pacific (Fig. 7b), consistent with

286 the surface wind EOF2 pattern (Fig. 1b). In the northwest section of the anomalous
287 WNP anticyclone, an anomalously north-eastward moisture transport prevails over
288 southern East Asia, thereby bringing more moisture to East Asia from the deep tropics.
289 For the meridional overturning circulation, the centre of the anomalous sinking
290 motion is shifted northward by approximately 10°N for the C-Mode compared to the
291 ENSO mode (Fig. 8b). Simultaneously for the C-Mode only, statistically significant
292 rising air anomalies appear on both sides of the equator at approximately $10^{\circ}\text{--}15^{\circ}\text{S}$
293 and $20^{\circ}\text{--}30^{\circ}\text{N}$ (Fig. 8b). The anomalous rising motion is much stronger north of the
294 equator, corresponding to large precipitation anomalies over southern China. Our
295 statistical analyses from Figures 4–8 suggest that the direct atmospheric response to
296 the ENSO mode is confined to the equatorial region, modifying the zonal atmospheric
297 circulation rather than the meridional circulation. The C-Mode acts to expand the
298 equatorial atmospheric anomalies towards off-equatorial regions. Therefore, ENSO
299 variability itself seems to have no significant impact on the East Asian climate; rather
300 it may affect the East Asian climate variability through its interaction with the annual
301 cycle of SST and lower tropospheric winds.

302

303 **4. Model Experiments**

304 According to our analysis of the observational data, we summarize that ENSO
305 without the presence of the C-Mode would give rise to very different atmospheric
306 circulation anomalies, especially over the WNP region. To verify this, two
307 experiments were designed. In the first set of experiments (EX_AC), the

308 ENSO-associated SST anomalies, obtained by the regression of monthly SST
309 anomalies upon the normalized PC1 (Fig. 1), are imposed on the climatological
310 annual cycle of SST in the entire tropics (20°S-20°N). Multiplying the SST anomaly
311 pattern by the normalized PC1 gives the spatiotemporal evolution of the SST anomaly
312 field. SST anomalies outside of the tropical bands are set to zero. The second
313 experiment (EX_NO_AC) has the same ENSO SST anomaly forcing but not the
314 annual cycle-associated meridional movements of climatological SSTs as boundary
315 forcing. The climatological SSTs are specified as the September equinox conditions
316 when the Sun is located directly over the equator. The EX_NO_AC experiment is
317 designed to investigate the importance of the SST annual cycle to ENSO associated
318 atmospheric circulation anomalies over the WNP through inter-comparison with the
319 EX_AC experiment. All simulations are integrated from 1958 to 2001, a period that
320 covers all the observed strong El Niño events except for the 2009/10 event. We
321 conduct a 10-member ensemble of the experiments.

322 Figure 9 shows the evolution of the total SST fields with and without inclusion
323 of the annual cycle, which are used to force the atmospheric model. The meridional
324 movement of the central Pacific SSTs during the 1997/98 El Niño event is taken as an
325 example to display the crucial difference arising from the two experiment designs. We
326 choose a zonal mean region near the dateline (160°–180°W) to display the SST
327 evolution, since the ENSO SST anomalies and the background SSTs are both
328 relatively strong here and hence can easily excite an atmospheric convection response.
329 For the experiment including the seasonal cycle (EX_AC), the maximum SSTs are

330 first found centered on the equator from June to October of 1997. Afterwards, the
331 maximum SSTs move abruptly into the Southern Hemisphere and become centered at
332 about 5°S (Fig. 9a). In contrast, in the experiment excluding the SST annual cycle
333 (EX_NO_AC), the maximum SSTs stay centered on the equator and display no
334 meridional movement for the entire 1997/98 El Niño event (Fig. 9b). Differences in
335 this SST latitude–time evolution clearly indicate that the southward shift of the total
336 SSTs is dependent on the seasonal cycle of climatological SST, which is very similar
337 to the observations (Zhang et al. 2015).

338 Figure 10 shows the composite surface wind anomalies during the strong El Niño
339 decaying phase for the observations and the two experiments. For the experiment
340 including the annual cycle of SST (EX_AC), the atmospheric model realistically
341 simulates two dominant observed features during the El Niño decaying phase: one is
342 the southward shift of the CP zonal wind anomalies and the other is the strong
343 anticyclonic circulation anomaly over the WNP region (Fig. 10a and b). This wind
344 anomaly pattern is very similar to that of EOF2 (Fig. 1b). In the northwestern section
345 of the anomalous WNP anticyclone, northeastward wind anomalies prevail over East
346 Asia, which bring more water vapor from the south to China (Figs. 10a and 7b). In
347 contrast to the EX_AC experiment, no obvious meridional movement of the CP zonal
348 wind anomalies is found in the EX_NO_AC experiment (Fig. 10c). In this experiment,
349 the cold and warm SST anomalies are, respectively, specified over the WNP and
350 Indian Ocean, which are argued to be important for the occurrence of the WNP
351 anticyclonic anomalies in previous studies (e.g., Wang et al. 2000; Xie et al. 2009).

352 However, no significant WNP anticyclonic circulation anomaly is seen in our
353 experiment when the annual cycle of SST is excluded (Fig. 10c). This shows that the
354 SST annual cycle is the crucial necessary condition for the development of the
355 anomalous low-level WNP circulation.

356 We also examine the sea-level pressure (SLP) anomaly evolution over the
357 Philippine Sea (10° – 20° N, 120° – 150° E) associated with strong El Niño events (Fig.
358 11), following the area definition of Wang et al. (2000). The observed Philippine Sea
359 SLP anomalies stay negative before the autumn season of El Niño developing phase
360 and then rapidly reverse their sign around September(0). Higher-than-normal SLP
361 anomalies over the Philippine Sea persist for three or four seasons into the El Niño
362 decaying summer (Fig. 11). The EX_AC experiment exhibits a similar Philippine Sea
363 SLP anomaly evolution to the observations. In contrast to the EX_AC experiment,
364 there are no positive SLP anomalies developing over the Philippine Sea in the
365 EX_NO_AC simulation. Figures 10 and 11 highlight the importance of the SST
366 annual cycle for the formation of the WNP anticyclonic anomalies during El Niño
367 conditions. Contrasting the atmospheric response in these two experiments, we expect
368 to find very different precipitation anomalies over eastern China. Indeed, in the
369 EX_AC experiment, we find that southern China receives stronger precipitation
370 anomalies during the El Niño decaying phase (Fig. 12a), consistent with the
371 observations (Fig. 3). Northern China experiences different precipitation anomalies
372 from the observations, possibly due to too strong impacts from the mid-latitudes in the
373 model and/or model biases in simulating the WNP circulation. However, in the

374 EX_NO_AC experiment, no statistically significant precipitation anomalies can be
375 found even over southern China (Fig. 12b), consistent with the absence of the
376 anomalous WNP anticyclonic circulation in this experiment. Comparisons of the two
377 modeling experiments verify our hypothesis that ENSO SST variability itself and its
378 associated circulation pattern, without interaction with the annual cycle (C-Mode),
379 cannot give rise to the observed WNP atmospheric circulation anomalies and their
380 associated precipitation anomalies over East Asia.

381

382 **5. Conclusions and Discussion**

383 Southern China usually receives enhanced precipitation during the decaying
384 phases of El Niño events and many studies have proposed various possible
385 mechanisms as to how ENSO affects the East Asian climate (e.g., Zhang et al. 1996;
386 Wang et al. 2000; Yang et al. 2007; Xie et al. 2009). In this study, we emphasize the
387 key role of the SST seasonal cycle in the genesis of the ENSO-related climate
388 anomalies over East Asia. It is shown that the direct (independent of the annual cycle)
389 atmospheric response to the ENSO mode does not generate any statistically
390 significant climate anomaly over East Asia, although it can give rise to climate
391 anomalies over the mid-latitude regions via atmospheric teleconnections (e.g., the
392 PNA pattern). In the tropical Pacific and adjacent continents, the direct ENSO signal
393 is confined to the equatorial region and does not expand meridionally towards, for
394 instance, the East Asian region. The C-Mode, resulting from the interaction between
395 interannual ENSO variability and the seasonal cycle of SST and circulation, is the

396 key player in enhancing precipitation over southern China during the decaying phase
397 of El Niño. As an important feature of the C-Mode, strong anticyclonic low-level
398 circulation anomalies are observed over the WNP region, which act to transport
399 warm and moist water vapor to East Asia from the equatorial oceanic region. Our
400 numerical model experiments reproduce well the key features of the anomalous
401 WNP circulation during the El Niño decaying phase when including the SST annual
402 cycle. However, no statistically significant WNP atmospheric circulation anomaly
403 and thus no precipitation anomalies over southern China are generated when the SST
404 boundary forcing is fixed to September equinox conditions (no annual cycle). As
405 mentioned previously, the C-mode provides the crucial bridge to bring ENSO
406 impacts to the off-equatorial region (e.g., southern China). Furthermore, we
407 emphasize that the C-Mode also provides a bridge in the spectral domain: the
408 impacts of ENSO in these regions are not only characterized by the interannual
409 ENSO timescale but most importantly by near-annual combination tones (see
410 discussion in Stuecker et al. 2013, 2015 for details). This key spectral feature of the
411 C-Mode has been overlooked in many previous climate impact studies by filtering
412 out the near-annual variability and only focusing on the interannual frequency band.

413 Previous studies proposed that the WNP SST cooling and delayed Indian Ocean
414 warming (both due to air/sea interaction) are the key mechanisms in forcing the WNP
415 anticyclonic circulation anomalies during the El Niño decaying phase (e.g., Wang et
416 al. 2000; Yang et al. 2007; Xie et al. 2009). In our simulations, the anomalous WNP
417 circulation cannot be produced when the annual cycle is omitted, although the WNP

418 SST cooling and Indian Ocean warming are included in the experimental SST
419 anomaly boundary forcing. Stuecker et al. (2015) argued that the WNP anticyclonic
420 circulation anomalies are predominantly a result of the southward shift of increased
421 convection anomalies, which could induce subsidence over the WNP through a
422 meridional circulation. In recent decades, steady progress has been made in
423 simulating the key observed features of El Niño (e.g., AchutaRao and Sperber 2002,
424 2006; Guilyardi 2006; Randall et al. 2007; Zhang et al. 2012). However, many studies
425 demonstrate the existence of systematic errors in the simulated mean state and annual
426 cycle (e.g., van Oldenborgh et al. 2005; Capotondi et al. 2006; Guilyardi 2006, 2009;
427 Wittenberg et al. 2006). These biases may cause large problems in simulating the
428 regional climate responses of El Niño, even if we simulate a relatively realistic El
429 Niño as defined by its anomalous evolution. This suggests that the climate community
430 should pay close attention to the simulation of both realistic ENSO variability and the
431 annual cycle in order to be able to simulate the El Niño-associated regional climate
432 anomalies.

433

434 **Acknowledgements:** This work is supported by the Special Fund for Public
435 Welfare Industry (Meteorology) (GYHY201506013, GYHY201406022), the
436 National Basic Research Program "973" (2012CB417403), and Jiangsu Provincial
437 Qinglan Project. The authors are grateful to research collaboration between
438 University of Reading Department of Meteorology and NUIST, which has provided
439 financial support to facilitate visits of WZ and AGT to respective institutes. AGT was

440 supported by the National Centre for Atmospheric Science.

441

442 **Reference**

- 443 AchutaRao, K., and K. R. Sperber, 2002: Simulation of the El Niño Southern
444 Oscillation: Results from the Coupled Model Intercomparison Project. *Clim. Dyn.*,
445 19, 191–209.
- 446 AchutaRao, K., and K. R. Sperber, 2006: ENSO simulation in coupled
447 ocean-atmosphere models: are the current models better? *Clim. Dyn.*, 27, 1–15.
- 448 Annamalai, H., P. Liu, and S.-P. Xie, 2005: Southwest Indian Ocean SST variability:
449 Its local effect and remote influence on Asian monsoons. *J. Climate*, 18,
450 4150–4167.
- 451 Ashok, K., S. K. Behera, S. A. Rao, H. Y. Weng, and T. Yamagata, 2007: El Niño
452 Modoki and its possible teleconnection. *J. Geophys. Res.*, 112, C11007,
453 doi:10.1029/2006JC003798.
- 454 Bjerknes, J., 1969: Atmospheric teleconnections from the equatorial Pacific. *Mon.*
455 *Wea. Rev.*, 97, 163–172.
- 456 Capotondi, A., A. Wittenberg, and S. Masina, 2006: Spatial and temporal structure of
457 tropical Pacific interannual variability in 20th century coupled simulations. *Ocean*
458 *Modell.*, 15, 274–298.
- 459 Charney, J. G. and J. Shukla, 1981: Predictability of monsoons. *Monsoon Dynamics*,
460 Editors: Sir James Lighthill and R. P. Pearce, Cambridge University Press, pp.
461 99–109.
- 462 Feng, J., L. Wang, W. Chen, S. K. Fong, and K. C. Leong, 2010: Different impacts of
463 two types of Pacific Ocean warming on Southeast Asia rainfall during boreal
464 winter. *J. Geophys. Res.*, 115, D24122, doi:10.1029/2010JD014761.
- 465 Feng, J., and J. Li, 2011: Influence of El Niño Modoki on spring rainfall over South
466 China. *J. Geophys., Res.*, 116, doi:10.1029/2010JD015160.
- 467 Fu, C. B., and X. L. Teng, 1988: Relationship between summer climate in China and
468 El Niño/Southern Oscillation phenomenon (in Chinese). *Chin. J. Atmos. Sci.*, 12,
469 133– 141.
- 470 Gill, A. E., 1980: Some simple solutions for heat-induced tropical circulation. *Quart. J.*

471 Roy. Meteor. Soc., 106, 447–462.

472 Guilyardi, E., 2006: El Niño-mean state-seasonal cycle interactions in a multi-model
473 ensemble. *Clim. Dyn.*, 26, 329–348.

474 Guilyardi, E., A. Wittenberg, A. Fedorov, M. Collins, C. Wang, A. Capotondi, G. J.
475 van Oldenborgh, and T. Stockdale, 2009: Understanding El Niño in
476 ocean-atmosphere general circulation models. *Bull. Am. Meteorol. Soc.*, 90,
477 325–340.

478 Harrison, D. E., 1987: Monthly mean island surface winds in the central tropical
479 Pacific and El Niño events. *Mon. Wea. Rev.*, 115, 3133–3145.

480 Harrison, D. E. and N. K. Larkin, 1996: The COADS sea level pressure signal: a
481 near-global El Niño composite and time series view, 1946-1993. *J. Climate*, 9,
482 3025–3055.

483 Harrison, D. E., and N. K. Larkin, 1998: EL Niño–Southern Oscillation sea surface
484 temperature and wind anomalies, 1946–1993. *Rev. Geophys.*, 36, 353–399.

485 Harrison, D. E., and G. A. Vecchi, 1999: On the termination of El Niño. *Geophys. Res.*
486 *Lett.*, 26, 1593–1596.

487 Huang, R. H., and Y. F. Wu, 1989: The influence of ENSO on the summer climate
488 change in China and its mechanism. *Adv. Atmos. Sci.*, 6, 21–32.

489 Kalnay, E., and Coauthors, 1996: The NCEP/NCAR 40-Year Reanalysis Project. *Bull.*
490 *Amer. Meteor. Soc.*, 77, 437–471.

491 Kao, H. Y., and J. Y. Yu, 2009: Contrasting eastern-Pacific and central-Pacific types of
492 ENSO. *J. Climate*, 22, 615–632.

493 Karori, M. A., J. Li, F.-F. Jin, 2013: The asymmetric influence of the two types of El
494 Niño and La Niña on summer rainfall over Southeast China. *J. Climate*, 26,
495 4567-4582.

496 Kug, J.-S., F.-F. Jin, and S.-I. An, 2009: Two types of El Niño events: Cold tongue
497 ElNiño and warm pool ElNiño. *J. Climate*, 22, 1499–1515.

498 Kug, J.-S., I.-S. Kang, and S.-I. An, 2003: Symmetric and antisymmetric mass
499 exchanges between the equatorial and off-equatorial Pacific associated with
500 ENSO. *J. Geophys. Res.-Oceans*, 108, doi:10.1029/2002JC001671.

501 Larkin, N. K., and D. E. Harrison, 2005: On the definition of El Niño and associated
502 seasonal average U.S. weather anomalies. *Geophys. Res. Lett.*, 32, L13705,
503 doi:10.1029/2005GL022738.

504 Lau, N.-C. and M. J. Nath, 2006: ENSO Modulation of the Interannual and
505 Intraseasonal Variability of the East Asian Monsoon - A Model Study. *J. Climate*,
506 19, 4508–4530, doi: <http://dx.doi.org/10.1175/JCLI3878.1>.

507 Lau, N.-C. and M. J. Nath, 2009: A Model Investigation of the Role of Air-Sea
508 Interaction in the Climatological Evolution and ENSO-Related Variability of the
509 Summer Monsoon over the South China Sea and Western North Pacific. *J.*
510 *Climate*, 22, 4771–4792, doi:10.1175/2009JCLI2758.1.

511 Lengaigne, M., J. Boulanger, C. Meinkes, and H. Spencer, 2006: Influence of the
512 seasonal cycle on the termination of El Niño events in a coupled general
513 circulation model. *J. Climate*, 19, 1850–1868.

514 Li, T., Y. C. Tung, and J. W. Hwu, 2005: Remote and local SST forcing in shaping
515 Asian-Australian monsoon anomalies. *J. Meteor. Soc. Japan*, 83, 153–167.

516 Matsuno, T., 1966: Quasi-geostrophic motion in the equatorial area. *J. Meteor. Soc.*
517 *Japan*, 44, 25–43.

518 McGregor, S., A. Timmermann, N. Schneider, M. F. Stuecker, and M. H. England,
519 2012, The effect of the South Pacific Convergence Zone on the termination of El
520 Niño events and the meridional asymmetry of ENSO. *J. Clim.*, 25, 5566–5586.

521 McGregor, S., N. Ramesh, P. Spence, M. H. England, M. J. McPhaden, and A.
522 Santoso, 2013, Meridional movement of wind anomalies during ENSO events and
523 their role in event termination. *Geophys. Res. Lett.*, 40, 749–754,
524 doi:10.1002/grl.50136.

525 Neelin, J. D., D. S. Battisti, A. C. Hirst, F.-F. Jin, Y. Wakata, T. Yamagata, and S. E.
526 Zebiak, 1998: ENSO theory. *J. Geophys. Res.*, 103, 14,261–14,290.

527 North, G. R., T. L. Bell, B. F. Cahalan, and F. J. Moeng, 1982: Sampling errors in the
528 estimation of Empirical Orthogonal Functions. *Mon. Weather Rev.*, 110, 699–706,

529 Ohba, M., and H. Ueda, 2009: Role of nonlinear atmospheric response to SST on the
530 asymmetric transition process of ENSO. *J. Climate*, 22, 177–192.

531 Randall, D. A., and Coauthors, 2007: Climate models and their evaluation. *Climate*
532 *Change 2007: The Physical Science Basis*, S. Solomon et al., Eds., Cambridge
533 University Press, 589–662.

534 Rayner, N. A., D. E. Parker, E. B. Horton, C. K. Folland, L. V. Alexander, D. P.
535 Rowell, E. C. Kent, and A. Kaplan, 2003: Global analyses of sea surface
536 temperature, sea ice, and night marine air temperature since the late nineteenth
537 century. *J. Geophys. Res.*, 108, 4407, doi:10.1029/2002JD002670.

538 Ren, H.-L., and F.-F. Jin, 2011: Niño indices for two types of ENSO. *Geophys. Res.*
539 *Lett.*, 38, L04704, doi:10.1029/2010GL046031.

540 Ropelewski, C. F., and M. S. Halpert, 1987: Global and regional scale precipitation
541 patterns associated with the El Niño/Southern Oscillation. *Mon. Wea. Rev.*, 115,
542 1606–1626.

543 Ropelewski, C. F., and M. S. Halpert, 1996: Quantifying Southern
544 Oscillation-precipitation relationships. *J. Climate*, 9, 1043–1059.

545 Spencer, H., 2004: Role of the atmosphere in seasonal phase locking of El Niño.
546 *Geophys. Res. Lett.*, 31, L24104, doi:10.1029/2004GL021619.

547 Stuecker, M. F., A. Timmermann, F.-F. Jin, S. McGregor, and H.-L. Ren, 2013: A
548 combination mode of the annual cycle and the El Niño/Southern Oscillation.
549 *Nature Geosci.*, 6, 540–544.

550 Stuecker, M., F.-F. Jin, A. Timmermann, and S. McGregor, 2015: Combination mode
551 dynamics of the anomalous North-West Pacific anticyclone. *J. Climate*, 28,
552 1093–1111.

553 Tao, S., and Y. Ding, 1981: Observational evidence of the influence of the
554 Qinghai-Xizang (Tibet) Plateau on the occurrence of heavy rain and severe
555 convective storms in China. *Bull. Amer. Meteor. Soc.*, 62, 23–30.

556 The GFDL Global Atmospheric Model Development Team, 2004: The New GFDL
557 Global Atmosphere and Land Model AM2-LM2: Evaluation with Prescribed SST
558 Simulations. *J. Clim.*, 17, 4641–4673.

559 Trenberth, K. E., and J. M. Caron, 2000: The Southern Oscillation revisited: Sea level
560 pressure, surface temperatures, and precipitation. *J. Climate*, 13, 4358–4365.

561 van Loon, H., and R. A. Madden, 1981: The Southern Oscillation. Part I: Global
562 associations with pressure and temperature in northern winter. *Mon. Wea. Rev.*,
563 109, 1150–1162.

564 van Oldenborgh, G. J., S. Philip, and M. Collins, 2005: El Niño in a changing climate:
565 A multi-model study. *Ocean Sci.*, 1, 81–95.

566 Vecchi, G., and D. E. Harrison, 2003: On the termination of the 2002–03 El Niño
567 event. *Geophys. Res. Lett.*, 30, 1964, doi:10.1029/2003GL017564.

568 Vecchi, G., and D. E. Harrison, 2006: The termination of the 1997/98 El Niño. Part I:
569 Mechanisms of oceanic change. *J. Climate*, 19, 2633–2646.

570 Wallace, J. M., E. M. Rasmusson, T. P. Mitchell, V. E. Kousky, E. S. Sarachik, and H.
571 Von Storch, 1998: On the structure and evolution of ENSO-related climate
572 variability in the tropical Pacific: Lessons from TOGA. *J. Geophys. Res.*, 103,
573 14,169–14,240.

574 Wang, B., and Q. Zhang, 2002: Pacific-East Asian Teleconnection. Part II: How the
575 Philippine Sea Anomalous Anticyclone is Established during El Niño
576 Development. *J. Climate*, 15, 3252–3265.

577 Wang, B., Q. Bao, B. Hoskins, G. Wu, and Y. Liu, 2008: Tibetan Plateau warming and
578 precipitation change in East Asia. *Geophys. Res. Lett.*, 35, L14702,
579 doi:10.1029/2008GL034330.

580 Wang, C., and X. Wang, 2013: Classifying El Niño Modoki I and II by different
581 impacts on rainfall in Southern China and typhoon tracks. *J. Clim.*, 26,
582 1322–1338.

583 Wang, B., B. Xiang, and J.-Y. Lee, 2013: Subtropical High predictability establishes a
584 promising way for monsoon and tropical storm predictions. *PNAS*, 110,
585 2718–2722.

586 Wang, B., R. Wu, and X. Fu, 2000: Pacific-East Asian teleconnection: How does
587 ENSO affect East Asian Climate? *J. Clim.*, 13, 1517–1536.

588 Watanabe, M., and F.-F. Jin, 2002: Role of Indian Ocean warming in the development
589 of Philippine Sea anticyclone during ENSO. *Geophys. Res. Lett.*, 29,
590 doi:10.1029/2001GL014318.

591 Watanabe, M. and F.-F. Jin, 2003: A Moist Linear Baroclinic Model: Coupled
592 Dynamical-Convective Response to El Niño. *J. Climate*, 16, 1121–1139.

593 Weng, H., K. Ashok, S. K. Behera, S. A. Rao, and T. Yamagata, 2007: Impacts of
594 recent El Niño Modoki on dry/wet conditions in the Pacific rim during boreal
595 summer. *Climate Dyn.*, 29, 113–129.

596 Wittenberg, A. T., A. Rosati, N. C. Lau, and J. J. Ploshay, 2006: GFDL’s CM2 global
597 coupled climate models. Part III: Tropical Pacific climate and ENSO. *J. Climate*,
598 19, 698–722.

599 Wu, B., T. Li, and T. Zhou, 2010: Relative contributions of the Indian Ocean and local
600 SST anomalies to the maintenance of the western North Pacific anomalous
601 anticyclone during the El Niño decaying summer. *J. Climate*, 23, 2974–2986.

602 Wu, G. X., and H. Liu, 1995: Neighborhood response of rainfall to tropical sea surface
603 temperature anomalies. Part I: Numerical experiment. *Chinese J. Atmos. Sci.*, 19,
604 422–434.

605 Wu, R., and B. P. Kirtman, 2007: Observed relationship of spring and summer East
606 Asian rainfall with winter and spring Eurasian snow. *J. Climate*, 20, 1285–1304

607 Wu, R., and Z. Z. Hu, 2003: Evolution of ENSO-related rainfall anomalies in East
608 Asia. *J. Climate*, 16, 3742–3758.

609 Wu, T.-W., Z.-A. Qian, 2010: The Relation between the Tibetan Winter Snow and the
610 Asian Summer Monsoon and Rainfall: An Observational Investigation. *J. Climate*,
611 16: 2038–2051.

612 Wu, Z. W., B. Wang, J. P. Li, and F.-F. Jin, 2009: An empirical seasonal prediction
613 model of the East Asian summer monsoon using ENSO and NAO. *J. Geophys.*
614 *Res.*, 114, D18120, doi:10.1029/2009JD011733.

615 Wu, Z., J. Li, Z. Jiang, T. Ma, 2012: Modulation of the Tibetan Plateau snow cover on
616 the ENSO teleconnections: From the East Asian summer monsoon perspective. *J.*
617 *Climate*, 25, 2481–2489.

618 Xiang, B., B. Wang, T. Li, 2013: A new paradigm for predominance of standing
619 Central Pacific Warming after the late 1990s. *Clim. Dyn.*, 41, 327–340.

620 Xie, F., J. Li, W. Tian, J. Feng, and Y. Huo, 2012: Signals of El Niño Modoki in the

621 tropical tropopause layer and stratosphere. *Atmos. Chem. Phys.*, 12 , 5259-5273.

622 Xie, F., J. Li, W. Tian, J. Zhang, and J. Shu, 2014: The impacts of two types of El
623 Niño on global ozone variations in the last three decades. *Adv. Atmos. Sci.*, 31,
624 1113-1126.

625 Xie, F., J. Li, W. Tian, Y. Li, J. Feng, 2014: Indo-Pacific warm pool area expansion,
626 Modoki Activity, and tropical cold-point tropopause temperature variations. *Sci.*
627 *Rep.*, 4, doi:10.1038/srep04552.

628 Xie, S. P., K. Hu, J. Hafner, H. Tokinaga, Y. Du, G. Huang, and T. Sampe, 2009:
629 Indian Ocean capacitor effect on Indo-Western Pacific climate during the summer
630 following El Niño. *J. Climate*, 22, 730–747.

631 Yang, J., Q. Liu, S. P. Xie, Z. Liu, and L. Wu, 2007: Impact of the Indian Ocean SST
632 basin mode on the Asian summer monsoon. *Geophys. Res. Lett.*, 34, L02708,
633 doi:10.1029/2006GL028571.

634 Ye, D., 1981: Some characteristics of the summer circulation over the Qinghai-Xizang
635 (Tibet) Plateau and its neighborhood. *Bull. Amer. Meteor. Soc.*, 62, 14–19.

636 Yuan, Y., S. Yang, and Z. Zhang, 2012: Different Evolutions of the Philippine Sea
637 Anticyclone between the Eastern and Central Pacific El Niño: Possible Effects of
638 Indian Ocean SST. *J. Climate*, 25, 7867–7883.

639 Yeh, S.-W., J.-S. Kug, B. Dewitte, M.-H. Kwon, B. P. Kirtman, and F.-F. Jin, 2009: El
640 Niño in a changing climate. *Nature*, 461, 511–514.

641 Zhang, R., A. Sumi, and M. Kimoto, 1996: Impacts of El Niño on the East Asian
642 monsoon: A diagnostic study of the '86/87 and '91/92 events. *J. Meteor. Soc.*
643 *Japan*, 74, 49–62.

644 Zhang, R., A. Sumi, and M. Kimoto, 1996: A diagnostic study of the impact of El
645 Niño on the precipitation in China. *Adv. Atmos. Sci.*, 16, 229–241.

646 Zhang, Y., T. Li, and B. Wang, 2004: Decadal change of the spring snow depth over
647 the Tibetan Plateau: The associated circulation and influence on the East Asian
648 summer monsoon. *J. Climate*, 17, 2780–2793.

649 Zhang, W., and F.-F. Jin, 2012: Improvements in the CMIP5 simulations of
650 ENSO-SSTA meridional width. *Geophys. Res. Lett.*, 39, L23704,

651 doi:10.1029/2012GL053588.

652 Zhang, W., F.-F. Jin, and A. Turner, 2014: Increasing autumn drought over southern
653 China associated with ENSO regime shift. *Geophys. Res. Lett.*, 41,
654 doi:10.1002/2014GL060130.

655 Zhang, W., F.-F. Jin, J. Li, and H.-L. Ren, 2011: Contrasting impacts of two-type El
656 Niño over the western North Pacific. *J. Meteor. Soc. Japan*, 89, 563–569.

657 Zhang, W., F.-F. Jin, J. X. Zhao, L. Qi, and H.-L. Ren, 2013: The possible influence of
658 a non-conventional El Niño on the severe autumn drought of 2009 in Southwest
659 China. *J. Clim.*, 26, 8392–8405.

660 Zhang W., H. Li, F.-F. Jin, M. Stuecker, A. Turner, and N. Klingamam, 2015: The
661 annual-cycle modulation of meridional asymmetry in ENSO’s atmospheric
662 response and its dependence on ENSO zonal structure, *J. Climate*,
663 doi:10.1175/JCLI-D-14-00724.1, published online.

664

665 **Figure Captions**

666 **Figure 1.** The leading two EOF spatial patterns (a, b) and their corresponding
667 normalized PC time series (c) of surface wind anomalies (m/s) over the tropical
668 Pacific. The EOF spatial patterns are obtained by the regression of normalized PCs on
669 the surface wind anomalies. Light (dark) yellow and blue shadings in (a, b) present
670 westerly and easterly anomalies exceeding the 90% (95%) confidence level,
671 respectively.

672 **Figure 2.** Composite monthly evolution of normalized PC1 (red dotted line) and
673 normalized PC2 (blue dotted line) for all El Niño events during the 1961-2012 period.
674 The abscissa indicates a 24-month period from January of year 0 to December of year
675 1.

676 **Figure 3.** (a) FMAM precipitation anomalies (contours in mm/month) regressed upon
677 the preceding normalized DJF PC1. (b) Composite FMAM precipitation anomalies
678 during the El Niño decaying phase for the period 1961–2012. Light (dark) shading
679 indicates where the regression coefficient exceeds the 90% (95%) confidence level.

680 **Figure 4.** (a) Correlation between the FMAM precipitation anomalies and the
681 preceding DJF PC1 time series. (b) Same as (a), but for partial correlation removing
682 linearly the impact of the preceding JFM PC2. Light (dark) shading indicates a
683 correlation coefficient exceeding the 90% (95%) confidence level.

684 **Figure 5.** (a) Correlation between the FMAM precipitation anomalies and the
685 preceding JFM PC2. (b) Same as (a), but for partial correlation removing linearly the
686 impact of preceding DJF PC1. Light (dark) shading indicates a correlation coefficient
687 exceeding the 90% (95%) confidence level.

688 **Figure 6.** Explained variance of FMAM precipitation (%) over East China by the
689 simultaneous PC1 (a), both simultaneous PC1 and PC2 (b), and their difference (c).
690 The contours indicate values of 10, 20, 30, and 40.

691 **Figure 7.** Vertically integrated moisture transport anomalies (vectors, $\text{kg m}^{-1} \text{s}^{-1}$) and

692 anomalies of its divergence (shading, $10^{-5} \text{ kg m}^{-2} \text{ s}^{-1}$) during FMAM partially
693 regressed upon the preceding normalized DJF PC1 (a) and JFM PC2 (b). Vertical
694 integration is performed over surface-300 hPa. Only values with a partial correlation
695 coefficient exceeding the 95% confidence level are shown.

696 **Figure 8.** Zonal mean (110° – 120° E) FMAM pressure velocity (contours in 10^{-2} Pa/s)
697 partially regressed upon the preceding normalized DJF PC1 (a) and JFM PC2 (b).
698 Light (dark) yellow and blue shadings indicate positive and negative partial
699 correlation coefficients exceeding the 90% (95%) confidence level, respectively.

700 **Figure 9.** Seasonal evolution of zonal mean (160° – 180° W) SST from June(0) to
701 June(1) during the 1997/98 El Niño event for the (a) EX_AC and (b) EX_NO_AC
702 experiments.

703 **Figure 10.** Composite FMAM surface wind anomalies during the El Niño decaying
704 phase for (a) observations, (b) EX_AC experiment, and (c) EX_NO_AC experiment.
705 Light (dark) yellow and blue shadings indicate westerly and easterly anomalies
706 exceeding the 90% (95%) confidence level, respectively.

707 **Figure 11.** Composite monthly evolution of sea-level pressure anomalies (hPa) over
708 the Philippine Sea (10° – 20° N, 120° – 150° E) during El Niño events.

709 **Figure 12.** Composite FMAM precipitation anomalies during the El Niño decaying
710 phase for the (a) EX_AC and (b) EX_NO_AC experiments. Light (dark) shading
711 denotes values exceeding the 80% (90%) confidence level.

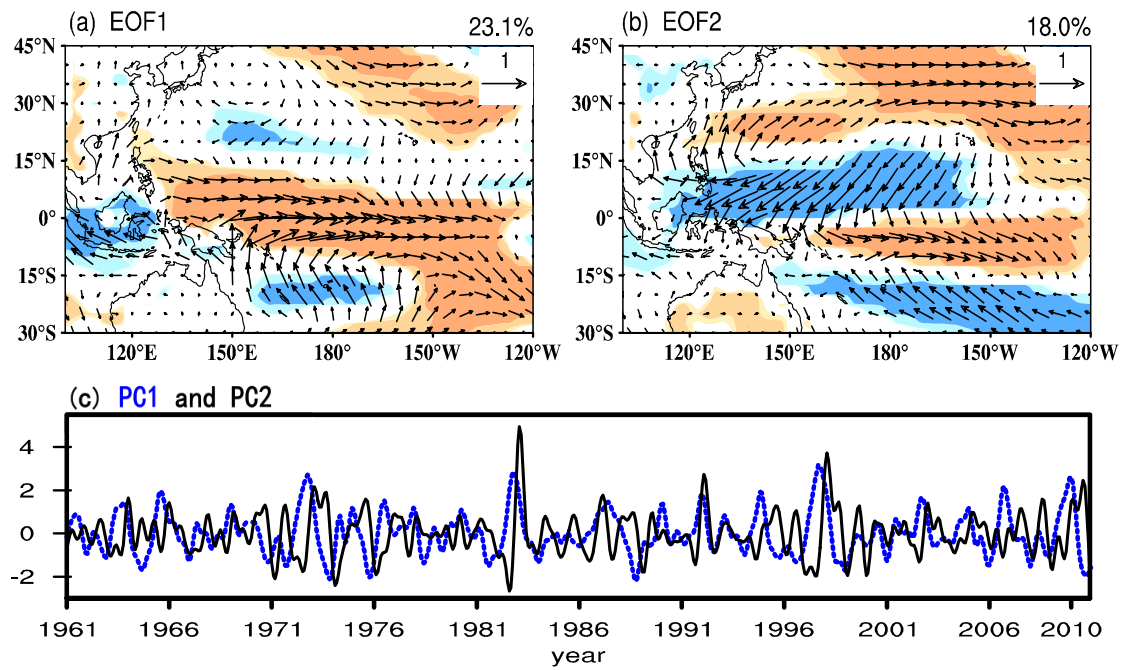


Figure 1. The leading two EOF spatial patterns (a, b) and their corresponding normalized PC time series (c) of surface wind anomalies (m/s) over the tropical Pacific. The EOF spatial patterns are obtained by the regression of normalized PCs on the surface wind anomalies. Light (dark) yellow and blue shadings in (a, b) present westerly and easterly anomalies exceeding the 90% (95%) confidence level, respectively.

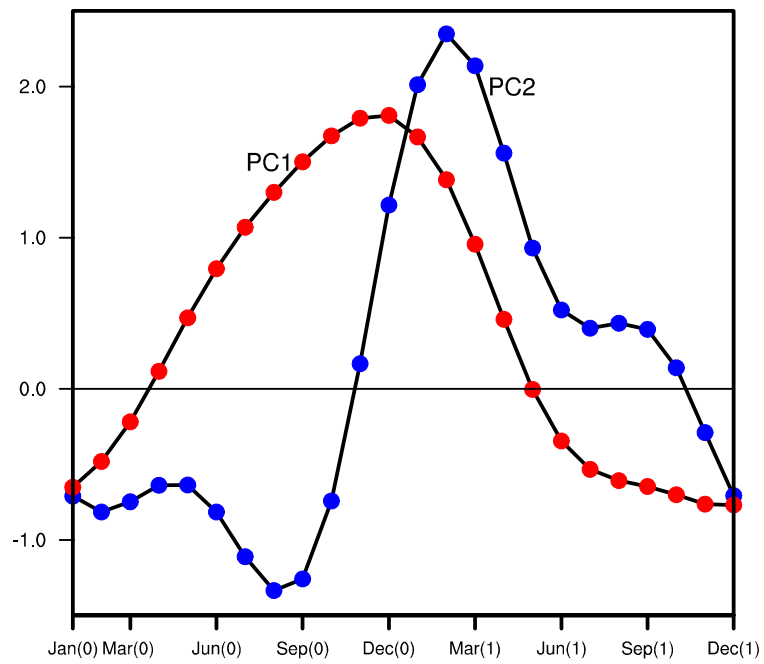


Figure 2. Composite monthly evolution of normalized PC1 (red dotted line) and normalized PC2 (blue dotted line) for all El Niño events during the 1961-2012 period. The abscissa indicates a 24-month period from January of year 0 to December of year 1.

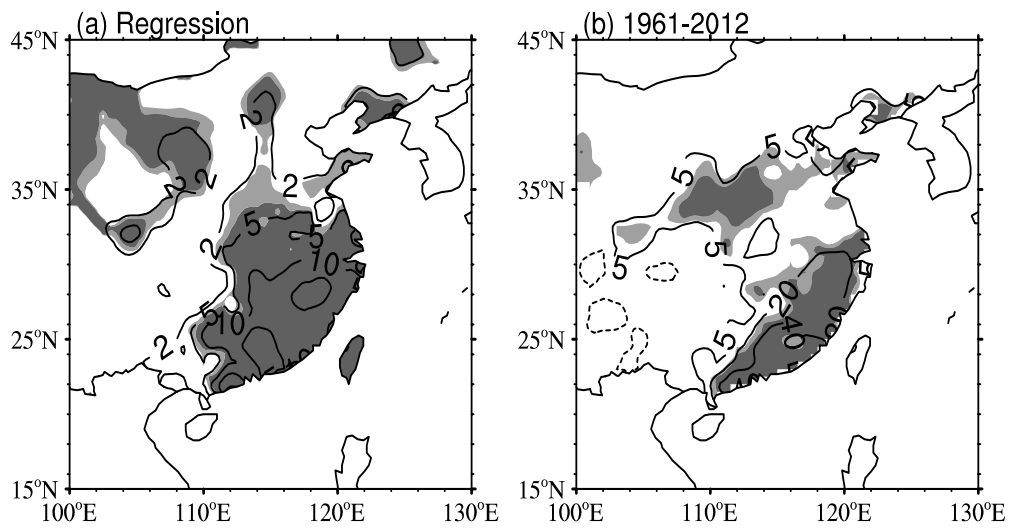


Figure 3. (a) FMAM precipitation anomalies (contours in mm/month) regressed upon the preceding normalized DJF PC1. (b) Composite FMAM precipitation anomalies during the El Niño decaying phase for the period 1961–2012. Light (dark) shading indicates where the regression coefficient exceeds the 90% (95%) confidence level.

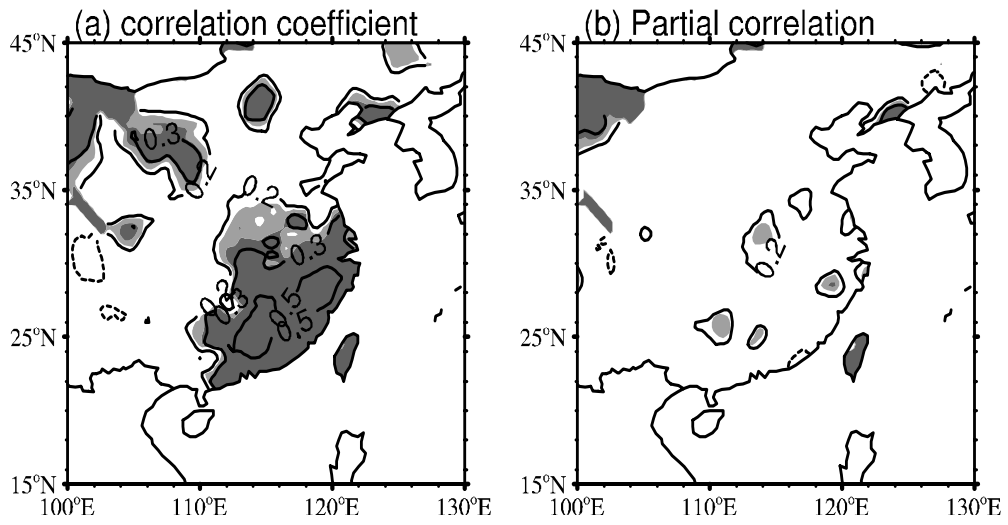


Figure 4. (a) Correlation between the FMAM precipitation anomalies and the preceding DJF PC1 time series. (b) Same as (a), but for partial correlation removing linearly the impact of the preceding JFM PC2. Light (dark) shading indicates a correlation coefficient exceeding the 90% (95%) confidence level.

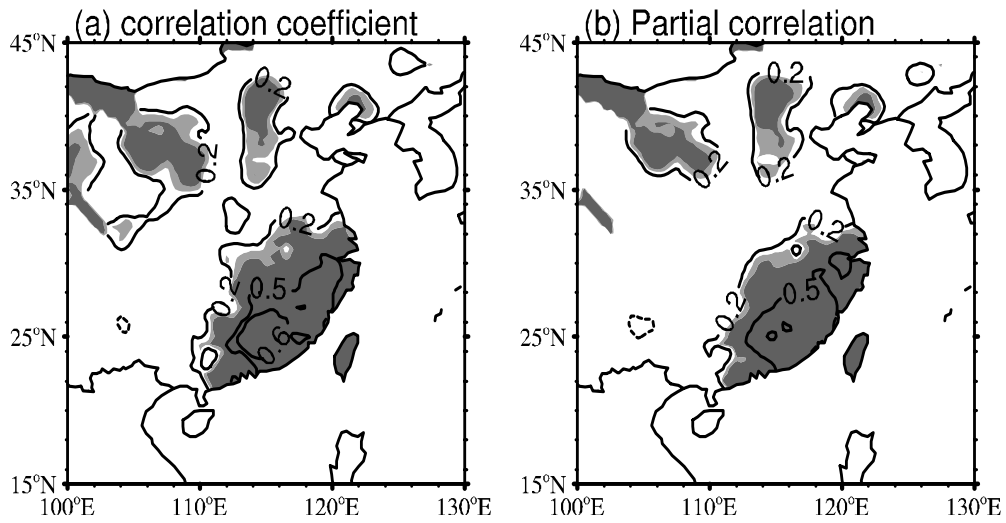


Figure 5. (a) Correlation between the FMAM precipitation anomalies and the preceding JFM PC2. (b) Same as (a), but for partial correlation removing linearly the impact of preceding DJF PC1. Light (dark) shading indicates a correlation coefficient exceeding the 90% (95%) confidence level.

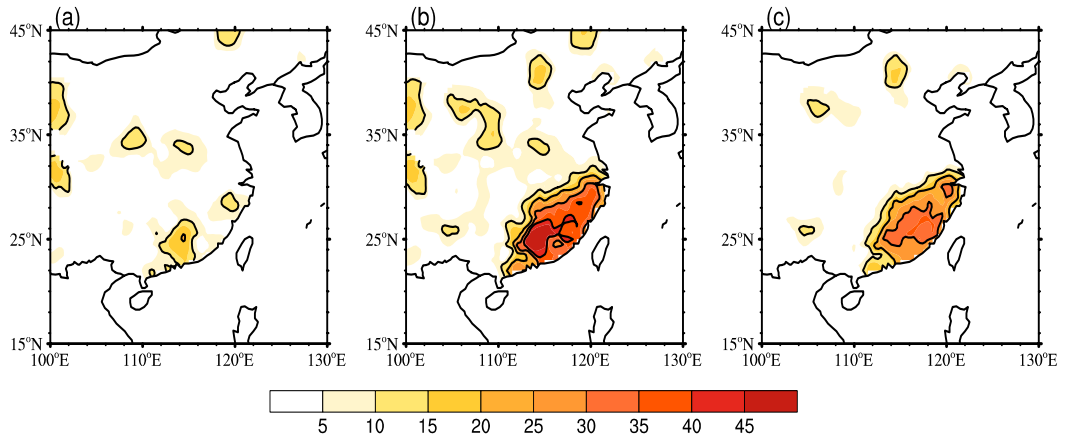


Figure 6. Explained variance of FMAM precipitation (%) over East China by the simultaneous PC1 (a), both simultaneous PC1 and PC2 (b), and their difference (c).

The contours indicate values of 10, 20, 30, and 40.

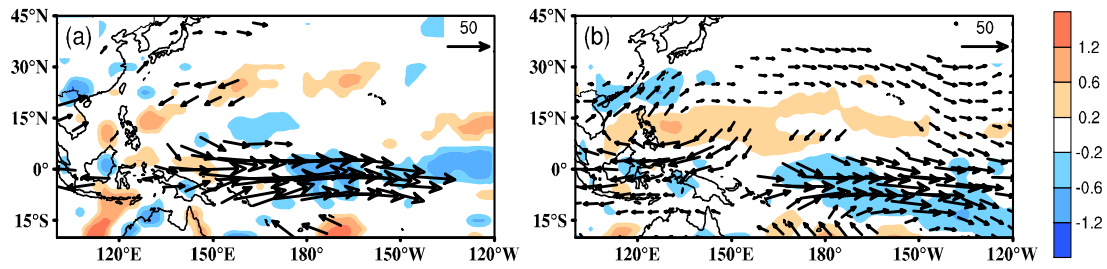


Figure 7. Vertically integrated moisture transport anomalies (vectors, $\text{kg m}^{-1} \text{s}^{-1}$) and anomalies of its divergence (shading, $10^{-5} \text{ kg m}^{-2} \text{ s}^{-1}$) during FMAM partially regressed upon the preceding normalized DJF PC1 (a) and JFM PC2 (b). Vertical integration is performed over surface-300 hPa. Only values with a partial correlation coefficient exceeding the 95% confidence level are shown.

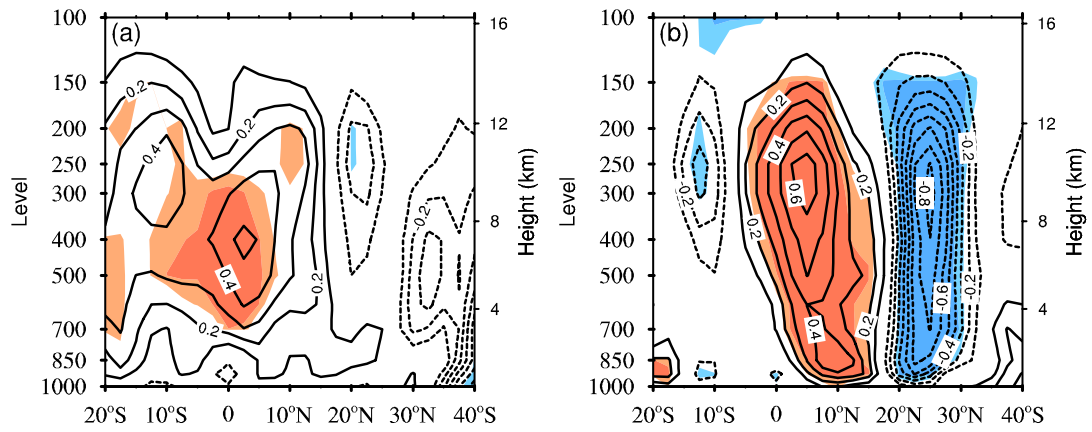


Figure 8. Zonal mean (110°–120°E) FMAM pressure velocity (contours in 10^{-2} Pa/s) partially regressed upon the preceding normalized DJF PC1 (a) and JFM PC2 (b). Light (dark) yellow and blue shadings indicate positive and negative partial correlation coefficients exceeding the 90% (95%) confidence level, respectively.

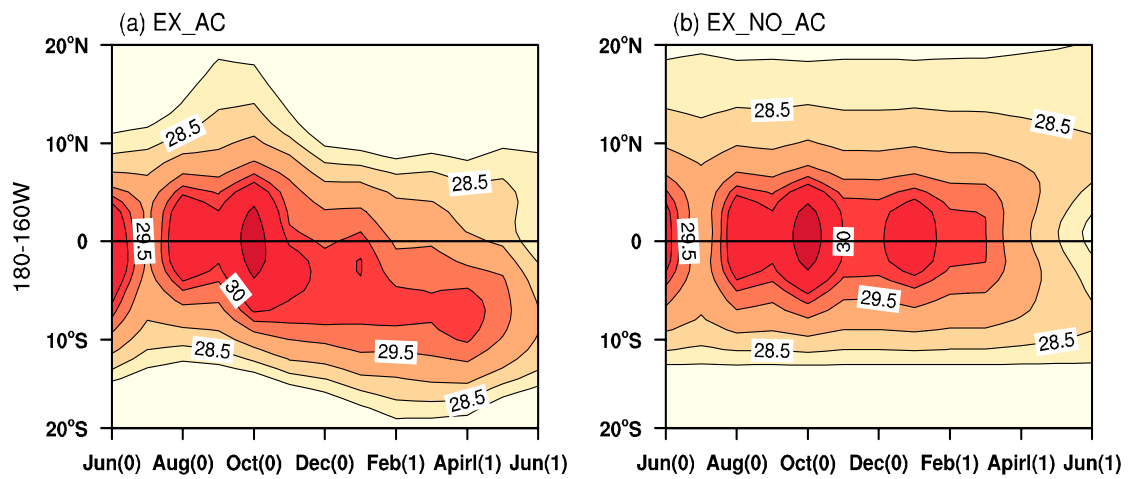


Figure 9. Seasonal evolution of zonal mean (160°–180°W) SST from June(0) to June(1) during the 1997/98 El Niño event for the (a) EX_AC and (b) EX_NO_AC experiments.

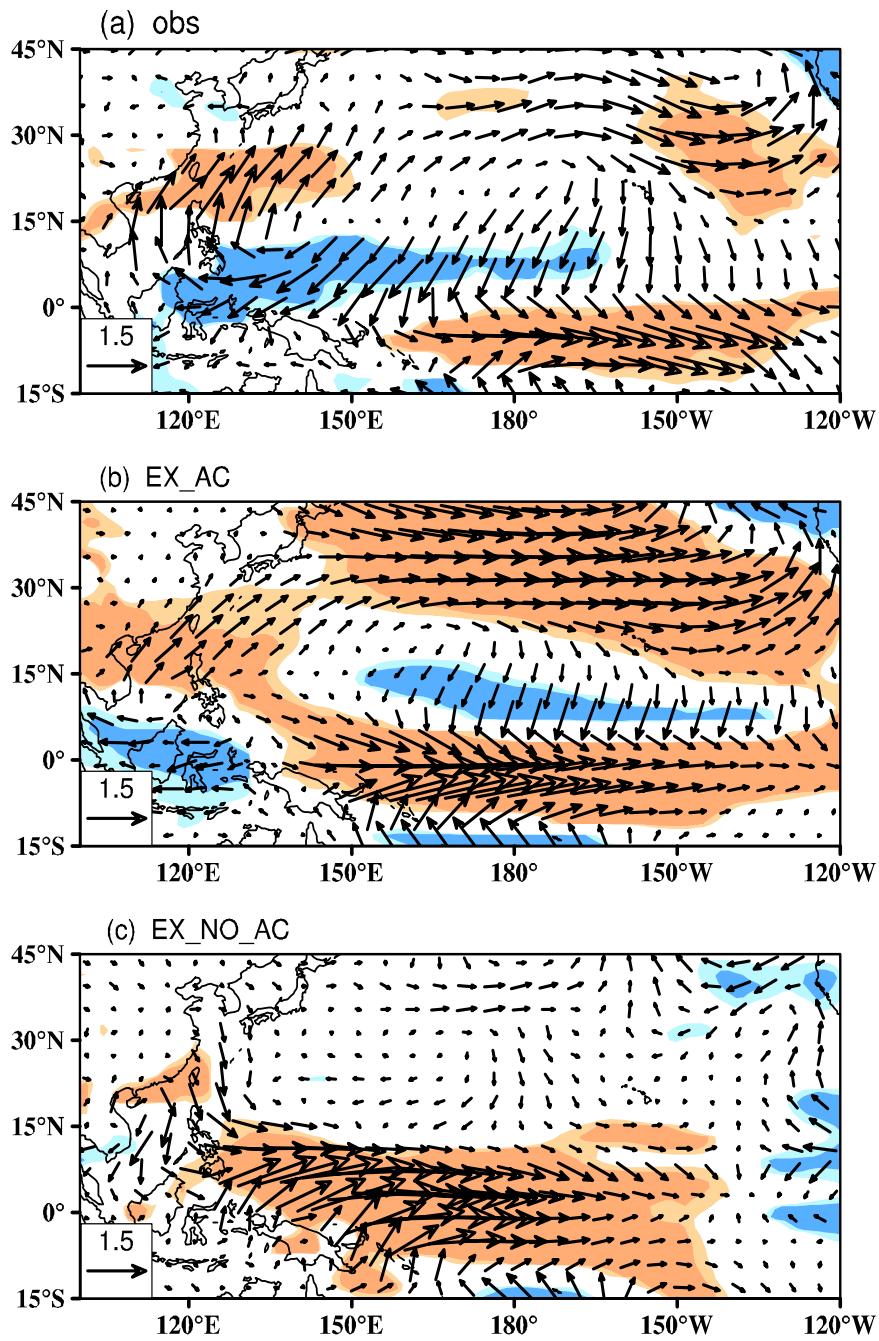


Figure 10. Composite FMAM surface wind anomalies during the El Niño decaying phase for (a) observations, (b) EX_AC experiment, and (c) EX_NO_AC experiment. Light (dark) yellow and blue shadings indicate westerly and easterly anomalies exceeding the 90% (95%) confidence level, respectively.

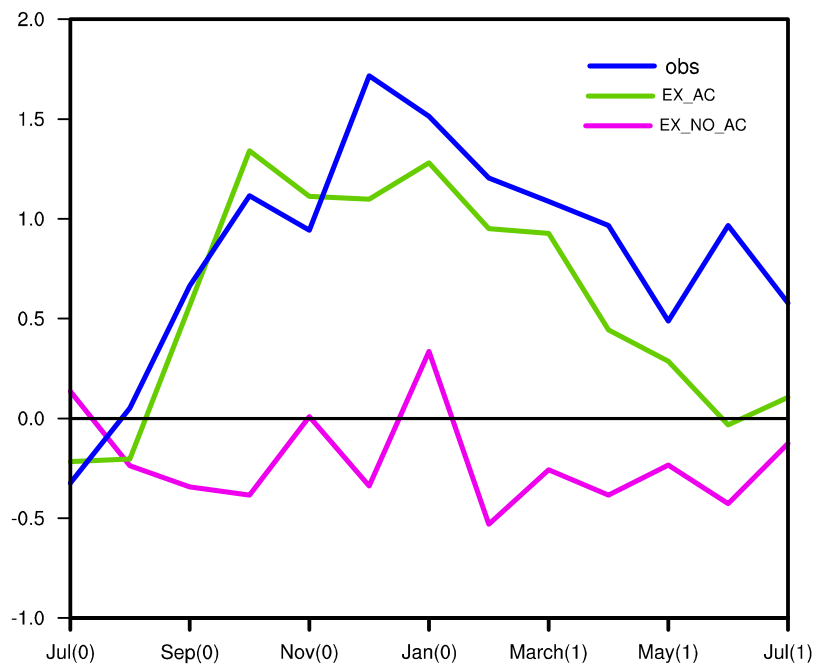


Figure 11. Composite monthly evolution of sea-level pressure anomalies (hPa) over the Philippine Sea (10° – 20° N, 120° – 150° E) during El Niño events.

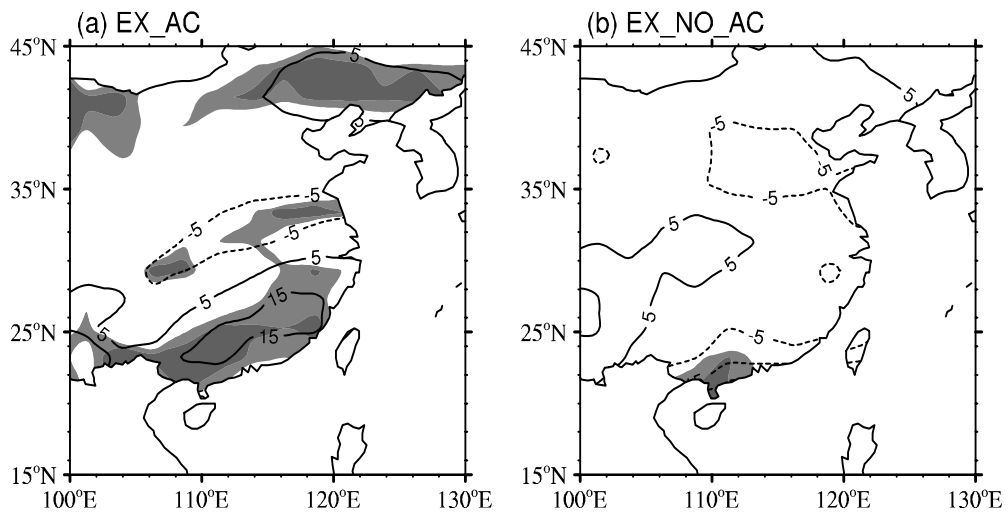


Figure 12. Composite FMAM precipitation anomalies during the El Niño decaying phase for the (a) EX_AC and (b) EX_NO_AC experiments. Light (dark) shading denotes values exceeding the 80% (90%) confidence level.